

# Monitoring the Opening and Recovery of the Blood–Brain Barrier with Noninvasive Molecular Imaging by Biodegradable Ultrasmall $\text{Cu}_{2-x}\text{Se}$ Nanoparticles

Hao Zhang,<sup>†</sup> Tingting Wang,<sup>†</sup> Weibao Qiu,<sup>‡</sup> Yaobao Han,<sup>†</sup> Qiao Sun,<sup>†</sup> Jianfeng Zeng,<sup>†</sup> Fei Yan,<sup>‡</sup> Hairong Zheng,<sup>‡</sup> Zhen Li,<sup>\*,†</sup> and Mingyuan Gao<sup>†</sup>

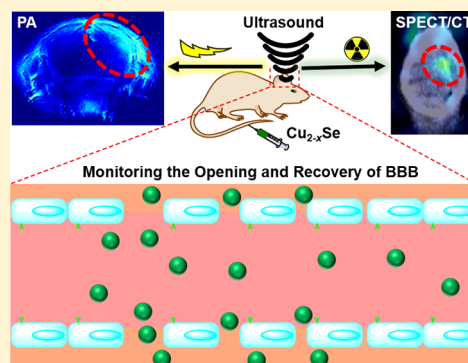
<sup>†</sup>Center for Molecular Imaging and Nuclear Medicine, State Key Laboratory of Radiation Medicine and Protection, School for Radiological and Interdisciplinary Sciences (RAD-X), Soochow University, Collaborative Innovation Center of Radiation Medicine of Jiangsu Higher Education Institutions, Suzhou 215123, PR China

<sup>‡</sup>Paul C. Lauterbur Research Center for Biomedical Imaging, Institute of Biomedical and Health Engineering, Shenzhen Institutes of Advanced Technology, Chinese Academy of Sciences, Shenzhen 518055, PR China

**S** Supporting Information

**ABSTRACT:** The reversible and controllable opening and recovery of the blood–brain barrier (BBB) is crucial for the treatment of brain diseases, and it is a big challenge to noninvasively monitor these processes. In this article, dual-modal photoacoustic imaging and single-photon-emission computed tomography imaging based on ultrasmall  $\text{Cu}_{2-x}\text{Se}$  nanoparticles (3.0 nm) were used to noninvasively monitor the opening and recovery of the BBB induced by focused ultrasound in living mice. The ultrasmall  $\text{Cu}_{2-x}\text{Se}$  nanoparticles were modified with poly(ethylene glycol) to exhibit a long blood circulation time. Both small size and long blood circulation time enable them to efficiently penetrate into the brain with the assistance of ultrasound, which resulted in a strong signal at the sonicated site and allowed for photoacoustic and single-photon emission computed tomography imaging monitoring the recovery of the opened BBB. The results of biodistribution, blood routine examination, and histological staining indicate that the accumulated  $\text{Cu}_{2-x}\text{Se}$  nanoparticles could be excreted from the brain and other major organs after 15 days without causing side effects. By the combination of the advantages of noninvasive molecular imaging and focused ultrasound, the ultrasmall biocompatible  $\text{Cu}_{2-x}\text{Se}$  nanoparticles holds great potential for the diagnosis and therapeutic treatment of brain diseases.

**KEYWORDS:** Ultrasmall  $\text{Cu}_{2-x}\text{Se}$  nanoparticles, focused ultrasound, blood–brain barrier, noninvasive molecular imaging



During the treatment of brain diseases, one big challenge is the efficient delivery of therapeutic agents across the blood–brain barrier (BBB), which is a specialized cerebral vascular system formed by brain endothelial cells and prevents more than 98% of drug molecules larger than ~400 Da in size from entering the brain.<sup>1,2</sup> To improve the delivery efficiency, great efforts have been devoted to developing different methods to overcome the BBB issue, including: (1) injection of hyperosmotic drug solutions,<sup>3,4</sup> (2) modification of drug structures for active efflux transporters,<sup>5,6</sup> (3) improvement of drug solubility to facilitate its penetration,<sup>7,8</sup> and (4) conjugation with targeting ligands (e.g., transferrin and angiopep-2) to enable active carrier-mediated transport across the BBB.<sup>9–11</sup> Although these methods resulted in promising outcomes, they have high risks of side effects or low delivery efficiency.

Recently, focused ultrasound (US) as a noninvasive technique has been used to deliver theranostic agents for the detection and treatment of various brain diseases, such as Alzheimer’s disease,<sup>12,13</sup> Parkinson’s disease,<sup>14,15</sup> and glioma.<sup>16,17</sup>

Ultrasound with a frequency below 1 MHz can induce noninvasive, reversible, and temporary opening of the BBB with the assistance of microbubbles (MB).<sup>18,19</sup> However, it is very challenging to noninvasively monitor and evaluate the permeability of the BBB after sonication. A number of imaging methods have been adopted for this purpose, such as contrast-enhanced magnetic resonance imaging (MRI),<sup>20–22</sup> fluorescence imaging,<sup>23</sup> and immunoelectron microscopy.<sup>24</sup>

The above methods have their own merits and disadvantages. For example, MRI has high resolution but with low sensitivity, and it usually takes a long time to obtain high-quality images. Fluorescence imaging has high sensitivity, but it is limited with respect to penetration and resolution due to the presence of the cranium and strong scattering in brain tissue. Immunoelectron microscopy cannot record real-time images of living tissue. The shortcomings of these imaging approaches

**Received:** May 4, 2018

**Revised:** July 1, 2018

**Published:** July 11, 2018

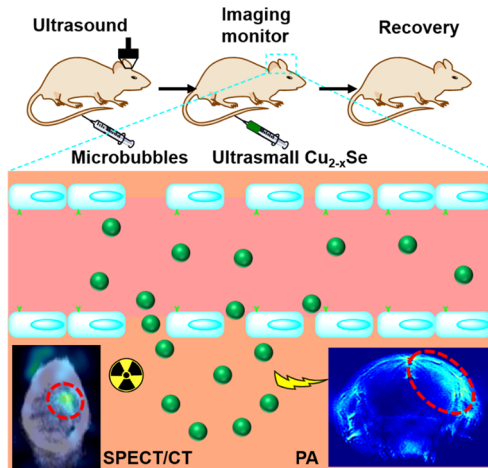
highlight the urgent need to develop an alternative method that has high sensitivity, high resolution, and deep penetration to allow the real-time monitoring of the opening and recovery of the BBB induced by localized ultrasound.

It is well-known that the performance of most imaging approaches is strongly dependent on the particular contrast agent. To achieve better noninvasive and real-time imaging of brain diseases, a variety of multifunctional nanomaterials have been reported.<sup>25–29</sup> For example, a core–shell multifunctional nanoprobe consisting of a gold particle core, a Raman-active layer, and a gadolinium-complex coating was used to delineate the margins of brain tumors in living mice before and during surgery through photoacoustic (PA) imaging, Raman imaging, and magnetic resonance imaging.<sup>27</sup>

It should be noted that most currently available nanoagents have a large particle size and short blood circulation time, and they cannot efficiently cross the BBB for better imaging and therapy. It also takes a long time for them to be completely degraded and excreted, casting a shadow on their biosafety. In contrast, ultrasmall multimodal nanotheranostics are more attractive and have shown great promise for biomedical imaging and disease therapy.<sup>30–33</sup> Their ultrasmall size gives them a long blood circulation half-life for efficient accumulation at the target organs<sup>34,35</sup> and fast degradation and excretion.<sup>36</sup>

In this work, <sup>99m</sup>Tc-labeled and unlabeled ultrasmall Cu<sub>2–x</sub>Se (UCS) nanoparticles (NPs) (3.0 ± 0.3 nm) with a long blood circulation half-life were used to monitor and evaluate ultrasound-induced temporary opening and recovery of the BBB of mice by dual-modal PA imaging and single-photon emission computed tomography (SPECT) imaging (Scheme 1). The results show that the BBB of mice can be opened by

**Scheme 1. Schematic Illustration of Dual-Modal Imaging Method for Monitoring the Opening and Recovery of the BBB Induced by Microbubble-Enhanced Ultrasound**



ultrasound and recovered after 2 h of sonication, and the ultrasmall nanoparticles were mainly accumulated at the interface between the hippocampus and the cortex. Moreover, the accumulated UCS NPs in the brain and other organs can be eliminated from the body within 2 weeks and do not cause serious toxicity, as evidenced by blood routine examinations and tissue-section staining. To our knowledge, this is the first report on the application of biodegradable ultrasmall nano-

particles for monitoring the ultrasound-induced opening and recovery of the BBB by versatile PA/SPECT imaging.

**Results and Discussion.** Focused US-mediated temporary opening of the BBB for the local delivery of therapeutic agents into the brain has been demonstrated to be a promising approach for the treatment of brain diseases. Noninvasively monitoring and evaluating the permeability of the BBB is a big challenge for this approach. To demonstrate the feasibility of opening the BBB with low-frequency ultrasound and assessing its permeability, Evans blue (EB) was selected to stain the brain tissue due to its very high affinity for serum albumin.<sup>37</sup> It was intravenously injected together with MB into the mice. As shown in Figure S1a, the opening of the BBB was successfully achieved by using 0.6 MPa acoustic pressure, as proved by the staining of sonicated brain with EB. In contrast, there was no opening of the BBB (i.e., the absence of EB stain) without MB (Figure S1a).

The above result demonstrates the importance of MB in US-mediated opening of the BBB. To assess the permeability and recovery of the opened BBB after sonication, the same dose of EB was intravenously injected via the tail veins of mice at different time points after the sonication. The mice were sacrificed at 2 h post-injection, and their brain slices are displayed in Figure S1b, which clearly shows the time-dependent gradual decrease of EB staining in the right brain. There is no obvious EB staining in the brain slice from the mouse injected with EB at 2 h after the sonication, which indicates the recovery of the opened BBB and that the EB–albumin complex cannot cross the recovered BBB.

The results from Figure S1 illustrate the feasibility of US-mediated temporary opening of the BBB and its recovery after 2 h. To noninvasively monitor the BBB opening and recovery process, spherical UCS NPs with a size of (3.0 ± 0.3) nm (Figures 1a and S2a) were synthesized as described elsewhere.<sup>35</sup> Their high-resolution TEM image (Figure 1a, inset) displays lattice fringes with an interplanar spacing of 0.20 nm, which matches well with that of the (220) planes of cubic berzelianite (Cu<sub>2–x</sub>Se). The average hydrodynamic size of UCS NPs is 13.5 nm, and the ζ potential is –10.1 mV (Figure S2b). These UCS NPs were confirmed to be cubic berzelianite (Cu<sub>2–x</sub>Se, JCPDS no. 06-0680) by their X-ray diffraction pattern (XRD, Figure S2c), with a Cu<sup>+</sup>-to-Cu<sup>2+</sup> ratio of 3.72, as determined by the X-ray photoelectron spectroscopy (XPS) spectrum of the Cu 2p orbital (Figure S2d). As mentioned previously, the ultrasmall NPs usually have a much-longer blood circulation half-life than larger ones. Notably, the UCS NPs exhibit a blood circulation half-life of 7.94 h (Figure 1b). The much-smaller size (3.0 ± 0.3 nm) and long blood circulation half-life indicate that these UCS NPs could efficiently cross the opened BBB induced by US and serve as an ideal imaging agent for monitoring the opening and recovery of the BBB by noninvasive PA imaging, because they exhibit a strong near-infrared (NIR) localized surface plasmon resonance (LSPR) (Figure S2e) and can efficiently convert NIR light into heat for PA imaging.<sup>38–40</sup> As shown in Figure S2f, the in vitro PA signals are linearly increased with the concentration of UCS NPs.

For in vivo application, PA imaging can overcome strong optical scattering and simultaneously retain a long penetration depth and good spatial resolution.<sup>41–44</sup> To monitor the opening of the BBB with UCS NPs through PA imaging, the mice were treated with US + MB + UCS in their right brain hemispheres, and a set of typical PA images of their brains

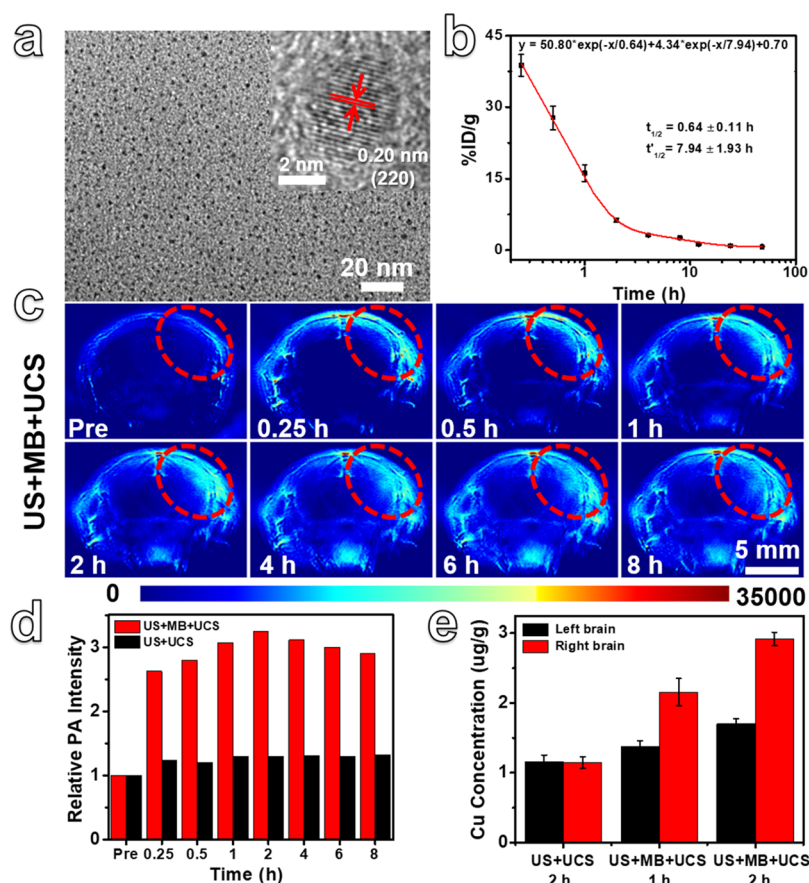


**Figure 1.** (a) TEM image of UCS NPs with an inset of a high-resolution TEM image. (b) Blood circulation half-time of UCS NPs in mice determined by measuring the Cu concentration with ICP-MS at different time points post-injection (dose: 5 mg/kg). (c) PA images of the mice brain before and after treatment with US + MB + UCS at different time points (dose: 5 mg/kg; the sonicated locations are indicated by the red circles). (d) Time-dependent relative PA intensity from the brain of the mice in the groups of US + MB + UCS and US + UCS. (e) The accumulation of UCS NPs at 1 and 2 h in the left and right brain of the mice from groups of US + MB + UCS and US + UCS, determined by ICP-MS.

collected at different times is shown in Figure 1c, in which the PA signals from the right hemisphere of the brain before treatment are very weak and then rapidly increase with the injection of UCS NPs after the opening of the BBB triggered by US + MB. The PA signals in the sonicated area reach their maximum after administration of UCS NPs for 2 h and then slightly decrease with the recovery of the opened BBB. The PA signals can be observed at a depth of 2.8 mm under the scalp of mice. In contrast, there is no obvious change in the right hemisphere of the brain at different time points in the US + UCS group of mice, which were sonicated without MB but injected with the same UCS NPs (Figure S3). The results indicate that the UCS NPs can cross the opened BBB triggered with US + MB but can hardly cross the unopened BBB.

To further highlight the changes in the sonicated brain region, the PA images of brains collected at different time points in the US + MB + UCS group were subtracted. Figure S4 shows two images (referred to as 2 h–precontrast and 8–2 h) from the subtraction of the image collected at precontrast and of the images collected at 2 and 8 h after the injection of UCS NPs. Obvious positive and negative enhancements are clearly observed in these two subtracted images. Quantitative analysis of the PA images from the US + MB + UCS group (Figure 1d) shows a significant enhancement in the right brain, and the maximum PA signals could be 3.2 times greater than that in the precontrast image. In contrast, the variation of PA

signals in the right brain from the US + UCS group is negligible.

To further demonstrate that the enhancement of PA signals is due to the penetration of UCS NPs into the brain through the opened BBB induced by US, the copper contents in the left and right brains of mice from both groups were quantified by inductively coupled plasma mass spectroscopy (ICP-MS). As demonstrated in Figure 1e, the Cu concentration in the right brain of mice from the US + MB + UCS group reached 2.9 μg/g at 2 h post-injection of UCS NPs, which is 2.6 times higher than that from the mice in the US + UCS control group (1.1 μg/g). In addition, the Cu concentration in the left brain is also slightly increased in the mice from the US + MB + UCS group, which suggests that the BBB in the left brain could be slightly influenced by the ultrasonic wave applied to the right brain.

As shown in Figure 1c,d, there is a slight decrease in PA signals obtained from 2 to 8 h, which could be attributed to the recovery of the opened BBB and the clearance of accumulated UCS NPs in the brain.<sup>45</sup> To verify the recovery of the opened BBB, the UCS NPs were injected into a mouse at 0.5 h after treatment with US + MB (referred to as US + MB + 0.5 h UCS). There is no obvious difference in the left and right brains in the precontrast image before injection of UCS NPs (Figure S5a), but enhanced contrast can be observed in the right hemisphere in PA images of the brain after injection of

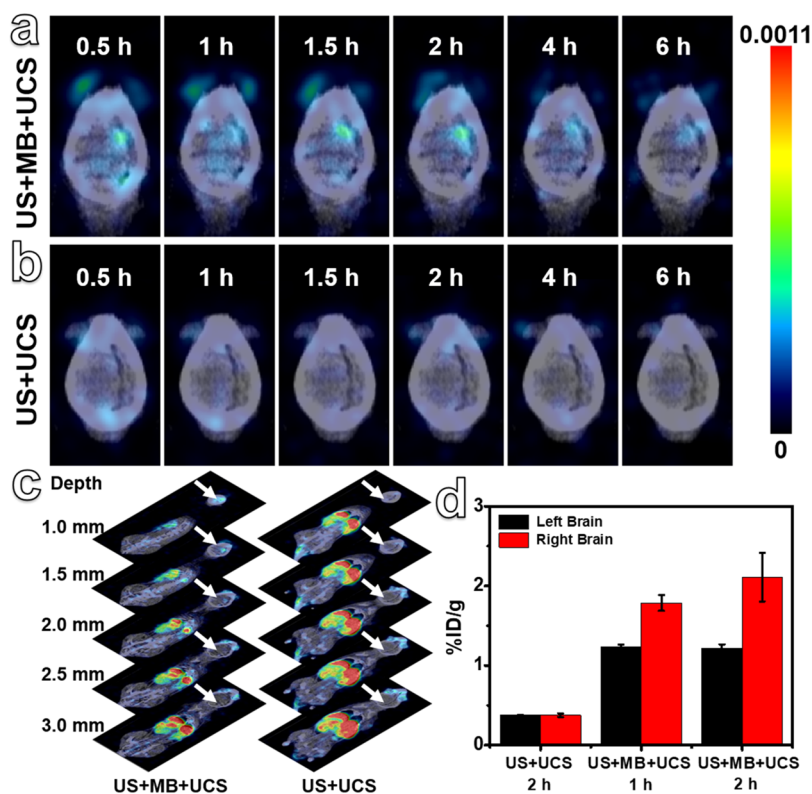


**Figure 2.** SPECT/CT images of the mice after treatment with a) US + MB + UCS-<sup>99m</sup>Tc and (b) US + UCS-<sup>99m</sup>Tc at different time points (dose: 5 mg/kg). (c) Whole-body SPECT/CT images of mice from the two groups at 2 h (with the sonicated locations indicated by the white arrows). (d) Accumulation of the UCS-<sup>99m</sup>Tc NPs in the left and right brains of mice from the US + MB + UCS-<sup>99m</sup>Tc and US + UCS-<sup>99m</sup>Tc groups, as determined by counting  $\gamma$  rays in the images collected at 1 and 2 h.

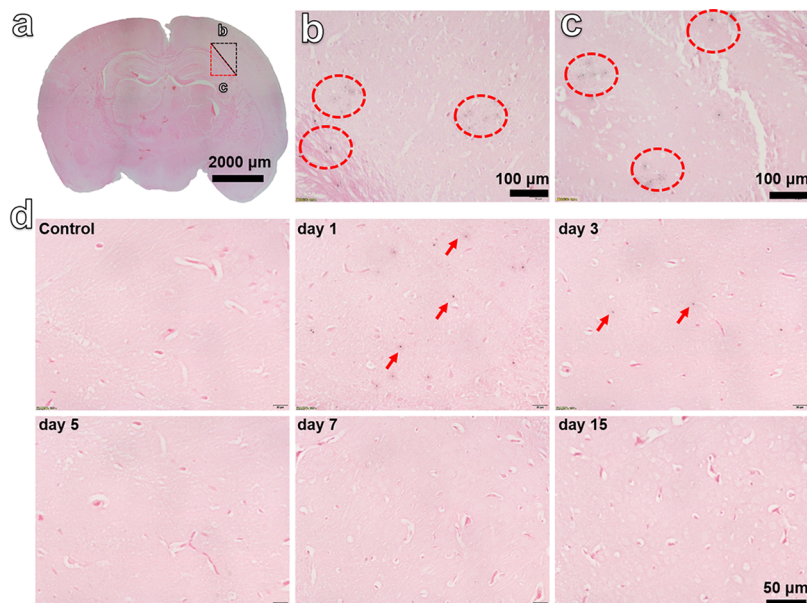


**Figure 3.** (a) Image of brain slice stained with rubeanic acid (RA) from a US + MB + UCS-treated mouse brain at 2 h (dose: 5 mg/kg). (b, c) Representative magnified photographs of the boxed area in panel a (with copper stains indicated by the red circles). (d) Images of brains stained with RA for the control and US + MB + UCS-treated mice excised at days 1, 3, 5, 7, and 15 (dose: 5 mg/kg; copper stains are indicated by the red arrows).

UCS NPs (Figure S5a). The maximum PA signal intensity (Figure S5b) is 2.2 times that of the precontrast image and lower than that of the US + MB + UCS group (i.e., 3.2 times). This result is consistent with that shown in Figure S1b, and supports the time-dependent recovery of the opened BBB.

The above results indicate a reversible opening of the BBB induced by US and MB, which can be monitored by the UCS NPs through their excellent PA imaging performance. To further demonstrate the US-mediated opening of the BBB, UCS NPs were chelated with radioactive <sup>99m</sup>Tc (referred to as

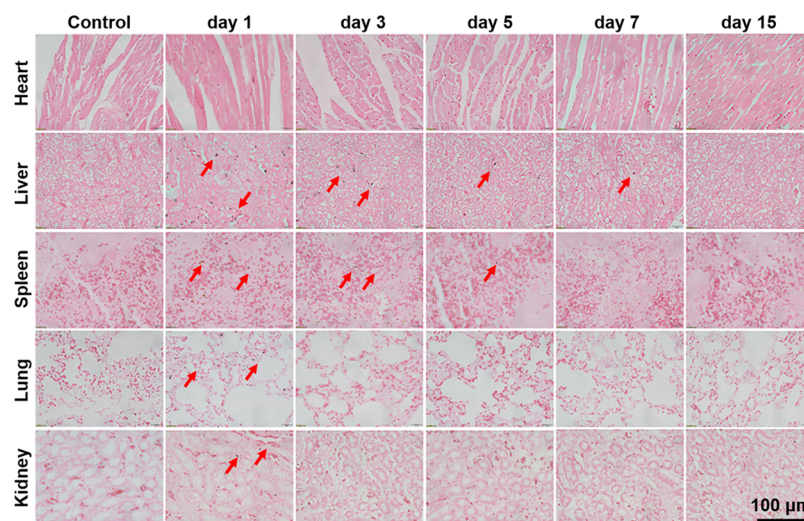


**Figure 4.** Images of heart, liver, spleen, lung, and kidney slices stained with RA for the control and US + MB + UCS-treated mice at days 1, 3, 5, 7, and 15 (dose: 5 mg/kg; copper stains are indicated by the red arrows).

UCS-<sup>99m</sup>Tc) through their surface multifunctional groups (–SH and –COOH) and then intravenously injected into mice with opened BBBs (treated with US + MB) for SPECT/computed tomography (CT) imaging. A series of SPECT/CT images were collected at different time points after injection. As shown in Figure 2a, strong  $\gamma$ -rays can be observed at the sonicated site in the brains of mice from the US + MB + UCS-<sup>99m</sup>Tc group. In contrast, there is no  $\gamma$ -emission from the brains of mice in the US + CS-<sup>99m</sup>Tc group (Figure 2b). Because SPECT/CT imaging has no penetration limitation, 0.5 mm-thick consecutive coronal slices through the whole mouse were obtained at 2 h to determine the penetration depth of the UCS-<sup>99m</sup>Tc NPs. The  $\gamma$  emissions can be observed at the depth of 2.5 mm under the skull, in contrast to the null signal at the sonicated site in the US + CS-<sup>99m</sup>Tc group without MB (Figure 2c).

An advantage of SPECT/CT imaging is the quantification of nanoparticle accumulation according to the intensity of  $\gamma$ -rays. The results in Figure 2d show that the accumulation of UCS-<sup>99m</sup>Tc NPs in the right hemisphere of the brain from the US + MB + UCS-<sup>99m</sup>Tc group is approximately 5-fold higher (2.1% ID/g) than that from the US + UCS-<sup>99m</sup>Tc group (0.4% ID/g). Similar to the results of ICP-MS (Figure 1e), the accumulation of UCS-<sup>99m</sup>Tc NPs in the left brain is also slightly higher than that in the brains of mice from the US + UCS-<sup>99m</sup>Tc group.

All of the imaging results demonstrate the penetration and accumulation of UCS NPs in the brain upon opening of the BBB. To further confirm the deposition of UCS NPs in the brain, the staining of brain tissues with rubeanic acid (RA) was performed. RA can interact with copper ions to form a dark compound, which can be clearly distinguished under the microscope.<sup>46,47</sup> As revealed in Figure 3a–c, marked copper staining in the cerebral cortex (Figure 3b) and hippocampus (Figure 3c) can be clearly seen, which illustrates that the UCS NPs can cross the opened BBB and be deposited in the brain. In contrast, there is no obvious copper staining in the brain of mice from the US + UCS group (Figure S6).

To qualitatively visualize the biodistribution and metabolism of the UCS NPs in the brain and other organs, the organs from healthy mice without any treatment and from mice in the US + MB + UCS group were excised and sectioned for RA staining.

Then, the residual organs were digested with HNO<sub>3</sub>/H<sub>2</sub>O<sub>2</sub> (2:1 = v/v) to quantitatively determine their copper concentration by ICP-MS measurements. As shown in Figure 3d, copper stains can be clearly observed in the hippocampus at day 1 and day 3, and then they decreased over time and were completely undetectable at day 7 and day 15. Furthermore, the ICP-MS results suggest that the Cu concentration in the brain is gradually reduced to the normal level at day 7 (Figure S7a), which demonstrates the biodegradation and metabolism of the accumulated UCS NPs in the brain.<sup>48</sup>

For the biodistribution of UCS NPs in other major organs (Figures 4 and S7a) of mice from the US + MB + UCS group, there are many copper stains in the liver and spleen at day 1, which is due to the rich phagocytes in the reticuloendothelial system (RES; Figure 4). The copper stains in both the liver and spleen are gradually reduced over time and have completely disappeared by 15 days after administration. Furthermore, the Cu concentration in the liver is drastically reduced with increasing culture time. In addition, the decreasing trend for the Cu concentration in the intestines is remarkably similar to that in the liver (Figure S7a), which indicates that the UCS NPs can be degraded and metabolized through the enterohepatic system.<sup>49</sup> Compared with the liver and spleen, only a few copper stains are observed in the slices from heart, lung, and kidney at day 1, and no copper stains are observed in them after 7 days. These results are consistent with the ICP-MS results (Figure S7a) and demonstrate that the UCS NPs can be easily and completely excreted from the mice by 15 days after administration.

To further evaluate whether the administrated UCS NPs cause any in vivo serious immune response after the mice are treated with US + MB + UCS, routine blood examinations were performed. This was because the side effects caused by a foreign substance could be reflected in hematological factors. As displayed in Figure S7b,c, the white blood cells (WBC) and platelets (PLT) are reduced on day 1 after treatment and then recover to the normal levels of the control mice on day 7 and day 15, which indicates a slight immune response.<sup>33,50</sup> Except for WBC and PLT, the other parameters (Figure S7d–i) show no physiologically significant difference between the mice from the US + MB + UCS-treated group and the control group.

Additionally, the major organs (brain, heart, liver, spleen, lung, and kidney) were collected and stained with hematoxylin and eosin (H&E) for histology analysis at day 15. The results in Figure S8 suggest that UCS NPs do not cause any tissue damage or inflammatory lesions compared to the control group. The low *in vivo* toxicity and relatively rapid clearance rate together with the advantages of dual-modal (PA/SPECT) imaging make the UCS NPs promising for the diagnosis and treatment of brain diseases with the assistance of focused US.

**Conclusions.** In conclusion, the opening of the BBB induced by microbubble-enhanced US and the recovery of the opened BBB were investigated using versatile dual-modal imaging with a therapeutic agent based on ultrasmall  $\text{Cu}_{2-x}\text{Se}$  NPs. The UCS nanoprobe exhibits a relatively long blood circulation half-life to enable the efficient crossing of the opened BBB and delivery into the brain to produce a strong photoacoustic signal for PA imaging and strong  $\gamma$ -rays for SPECT/CT imaging after being labeled with radioactive  $^{99\text{m}}\text{Tc}$ , which allows us to evaluate the ultrasound-induced temporary opening and recovery of the BBB in a noninvasive way. In addition, the UCS nanoprobe exhibits excellent biodegradability and biocompatibility, and they were completely degraded *in vivo* and metabolized within 15 days without serious side effects. Our work highlights the promising potential of ultrasmall  $\text{Cu}_{2-x}\text{Se}$  NPs for the imaging and therapy of brain diseases with the assistance of US in the future.

**Experimental Section. Materials.**  $\text{CuCl}_2 \cdot 2\text{H}_2\text{O}$  ( $\geq 99\%$ ), Se powder ( $-100$  mesh,  $\geq 99.5\%$ ), sodium borohydride ( $\text{NaBH}_4$ ,  $99\%$ ), and mercaptosuccinic acid (MSA,  $99\%$ ) were purchased from Sigma-Aldrich. Dimercapto poly(ethylene glycol) (HS-PEG-SH, MW = 5000) was purchased from Adamas. Milli-Q water ( $18 \text{ M}\Omega\text{-cm}$ ) was used in the experiments. All chemicals and reagents were used as received without any further purification.

**Synthesis of Ultrasmall  $\text{Cu}_{2-x}\text{Se}$  Nanoparticles.** In a typical synthesis, Se powder ( $0.5 \text{ mmol}$ ) was reduced by  $\text{NaBH}_4$  ( $1.5 \text{ mmol}$ ) in  $50 \text{ mL}$  of  $\text{H}_2\text{O}$  under magnetic stirring at room temperature under nitrogen protection. Then,  $5 \text{ mL}$  of aqueous solution of  $\text{CuCl}_2 \cdot 2\text{H}_2\text{O}$  ( $1 \text{ mmol}$ ) and MSA ( $6.66 \text{ mmol}$ ) was added into the selenium precursor solution under magnetic stirring, and the reaction mixture was kept under stirring for  $2 \text{ h}$ . The resultant black solution was centrifuged with a  $30 \text{ kDa}$  ultrafiltration tube at  $4000 \text{ rpm}$  to remove the excessive MSA, and HS-PEG-SH ( $0.04 \text{ mmol}$ ) was added to modify the surfaces of the  $\text{Cu}_{2-x}\text{Se}$  NPs at room temperature. The obtained ultrasmall  $\text{Cu}_{2-x}\text{Se}$  NPs (i.e., UCS NPs) were purified by a similar ultrafiltration method to remove the free HS-PEG-SH. The purification process was typically repeated three times using Milli-Q water as eluent.

**Characterization.** TEM images were captured using a FEI Tecnai G20 transmission electron microscope operating at an acceleration voltage of  $200 \text{ kV}$ . Dynamic light scattering (DLS) and  $\zeta$  potential measurements were conducted at  $25 \text{ }^\circ\text{C}$  on a Malvern Zetasizer Nano ZS90 equipped with a solid-state He-Ne laser ( $\lambda = 633 \text{ nm}$ ). The crystal structure of the UCS NPs was characterized with a Shimadzu XRD-6000 X-ray diffractometer equipped with  $\text{Cu K}\alpha_1$  radiation ( $\lambda = 0.15406 \text{ nm}$ ). XPS measurements were carried out on a Thermo Scientific Sigma Probe instrument using  $\text{Al K}\alpha$  X-ray radiation and fixed analyzer transmission mode. Ultraviolet–visible–near-infrared (UV–vis–NIR) spectra were collected on a PerkinElmer Lambda 750 UV–vis–NIR spectrophotometer.

**BBB Opening and Evans Blue Evaluation.** A US transducer ( $0.5 \text{ MHz}$  and  $30 \text{ mm}$  diameter) was used to temporarily open the BBB, driven by a function generator connected to a power amplifier. A removable cone filled with degassed water was employed to hold the transducer and guide the US beam into the brain. The acoustic parameters used were  $0.6 \text{ MPa}$  acoustic pressure,  $0.5 \text{ MHz}$  frequency,  $1 \text{ ms}$  pulse interval, and  $90 \text{ s}$  sonication duration. A total of  $50 \mu\text{L}$  of microbubbles (mean diameter of about  $2 \mu\text{m}$  and concentration of about  $1 \times 10^9$  bubbles/mL) were intravenously injected into mice before sonication. To confirm the successful opening of the BBB and its recovery, the mice were administered with EB dye ( $30 \text{ mg/kg}$ ) via the tail vein at different time points post-injection ( $0, 0.5, 1, \text{ and } 2 \text{ h}$ ) and then sacrificed at  $2 \text{ h}$  after EB injection.

**Blood Circulation Behavior.** Healthy BALB/c mice ( $n = 5$ ) were administered with the UCS NPs through the tail vein. Then, blood samples were collected from the retinal vein at  $0.25, 0.5, 1, 2, 4, 6, 8, 12, 24, \text{ and } 48 \text{ h}$ , respectively. The blood samples were digested with  $\text{HNO}_3/\text{H}_2\text{O}_2$  ( $2:1 = \text{v/v}$ ) for quantification of Cu by ICP-MS. The decay curve of the Cu concentration in the blood was fitted with a two-compartment model to determine the blood half-life.

**In Vivo PA Imaging.** PA imaging was performed with a Multispectral optoacoustic tomography scanner (MSOT, iThera Medical). For *in vivo* PA imaging, nude mice were anesthetized with  $1.5\%$  isoflurane delivered via a nose cone. Next, the UCS NPs (dose:  $5 \text{ mg/kg}$ ) were intravenously injected into the mice after treatment with US + MB (sonication:  $90 \text{ s}$ , MB:  $50 \mu\text{L}$ ) or US (sonication:  $90 \text{ s}$  without MB). The PA images of the mice were captured at different time points.

**In Vivo SPECT/CT Imaging.** Radioactive Technetium-99m (purchased from Shanghai GMS Pharmaceutical Co., Ltd.) with radioactivity of  $1 \text{ mCi}$  was added into the UCS NP solution ( $500 \mu\text{g/mL}$ ,  $200 \mu\text{L}$ ) in the presence of  $20 \mu\text{L}$  of stannous chloride ( $\text{SnCl}_2$ ,  $1 \text{ mg/mL}$  in  $0.1 \text{ M HCl}$ ) and then stirred gently for  $0.5 \text{ h}$  at room temperature. The obtained  $^{99\text{m}}\text{Tc}$ -labeled UCS NP solution was purified by ultrafiltration to remove free  $^{99\text{m}}\text{Tc}$ . The obtained UCS- $^{99\text{m}}\text{Tc}$  NPs were intravenously injected into the nude mice after treatment with US + MB (sonication:  $90 \text{ s}$ , MB:  $50 \mu\text{L}$ ) or US (sonication:  $90 \text{ s}$  without MB). The SPECT/CT images of mice were captured at different time points.

**In Vivo Metabolism and Toxicity Evaluation of the UCS NPs.** Healthy BALB/c mice were divided into 6 groups ( $n = 5$  in each group). The experimental groups were injected with the UCS NPs (dose:  $5 \text{ mg/kg}$ ) through the tail vein after treatment with US + MB (sonication:  $90 \text{ s}$ , MB:  $50 \mu\text{L}$ ). The healthy mice without any treatment were used as the control. Blood samples and major organs were collected and weighed at different time points (day 1, 3, 5, 7, and 15). Then, the blood routine was measured. Parts of the main organs (brain, heart, liver, spleen, lung, and kidney) were harvested and fixed using  $4\%$  paraformaldehyde. Tissue samples were then embedded in paraffin, sliced, and stained using RA and H&E. The rest of the organs were digested with  $\text{HNO}_3/\text{H}_2\text{O}_2$  ( $2:1 = \text{v/v}$ ) for quantification of Cu by ICP-MS.

## ■ ASSOCIATED CONTENT

### 📄 Supporting Information

The Supporting Information is available free of charge on the ACS Publications website at DOI: [10.1021/acs.nanolett.8b01818](https://doi.org/10.1021/acs.nanolett.8b01818).

Figures showing Evans blue staining of mouse brains, characterization of UCS NPs; PA images of the mice brain before and after treated with US + UCS, subtraction of PA images; PA images of mouse brains; images of brain slices stained with RA; time-dependent biodistribution and blood routine examinations; and histological staining of mouse brain, heart, liver, spleen, lung, and kidney slices. (PDF)

## AUTHOR INFORMATION

### Corresponding Author

\*E-mail: zhenli@suda.edu.cn.

### ORCID

Fei Yan: 0000-0003-4874-9582

Zhen Li: 0000-0003-0333-7699

Mingyuan Gao: 0000-0002-7360-3684

### Author Contributions

H.Z. did experiments, collected and analyzed data, and wrote the paper. T.W. and Y.H. performed the synthesis and characterization of UCS nanoparticles. W.Q., F.Y., and H.Z. provided the ultrasonic machines and discussion. Q.S. and J.Z. analyzed data and discussion. M.G. and Z.L. designed the experiments and wrote the paper.

### Notes

The authors declare no competing financial interest.

## ACKNOWLEDGMENTS

Z. Li acknowledges support from the National Natural Science Foundation of China (grant nos. 81471657 and 81527901), the 1000 Plan for Young Talents, Jiangsu Specially Appointed Professorship, and the Program of Jiangsu Innovative and Entrepreneurial Talents. H. Zheng is grateful to the support from National Key Basic Research Program of China (Grant No. 2015CB755500). F. Yan also acknowledges the support from Shenzhen Science and Technology Innovation Committee (Grant No. JCYJ20170413100222613). The authors also are grateful for support from the Jiangsu Provincial Key Laboratory of Radiation Medicine and Protection, the Priority Academic Development Program of Jiangsu Higher Education Institutions (PAPD).

## REFERENCES

- Armulik, A.; Genové, G.; Mãe, M.; Nisancioglu, M. H.; Wallgard, E.; Niaudet, C.; He, L.; Norlin, J.; Lindblom, P.; Strittmatter, K.; Johansson, B. R.; Betsholtz, C. *Nature* **2010**, *468*, 557–561.
- Ben-Zvi, A.; Lacoste, B.; Kur, E.; Andreone, B. J.; Mayshar, Y.; Yan, H.; Gu, C. *Nature* **2014**, *509*, 507–511.
- Brown, R. C.; Egleton, R. D.; Davis, T. P. *Brain Res.* **2004**, *1014*, 221–227.
- Doolittle, N. D.; Miner, M. E.; Hall, W. A.; Siegal, T.; Hanson, E. J.; Osztie, E.; McAllister, L. D.; Bubalo, J. S.; Kraemer, D. F.; Fortin, D.; Nixon, R.; Muldoon, L. L.; Neuwelt, E. A. *Cancer* **2000**, *88*, 637–647.
- Groothuis, D. R. *Neuro-Oncology* **2000**, *2*, 45–59.
- Rice, A.; Liu, Y.; Michaelis, M. L.; Himes, R. H.; Georg, G. I.; Audus, K. L. *J. Med. Chem.* **2005**, *48*, 832–838.
- Kabanov, A. V.; Batrakova, E. V.; Miller, D. W. *Adv. Drug Delivery Rev.* **2003**, *55*, 151–164.
- Singh, A.; Kim, W.; Kim, Y.; Jeong, K.; Kang, C. S.; Kim, Y.; Koh, J.; Mahajan, S. D.; Prasad, P. N.; Kim, S. *Adv. Funct. Mater.* **2016**, *26*, 7057–7066.
- Ying, X.; Wang, Y.; Liang, J.; Yue, J.; Xu, C.; Lu, L.; Xu, Z.; Gao, J.; Du, Y.; Chen, Z. *Angew. Chem., Int. Ed.* **2014**, *53*, 12436–12440.
- Ni, D.; Zhang, J.; Bu, W.; Xing, H.; Han, F.; Xiao, Q.; Yao, Z.; Chen, F.; He, Q.; Liu, J.; Zhang, S.; Fan, W.; Zhou, L.; Peng, W.; Shi, J. *ACS Nano* **2014**, *8*, 1231–1242.
- Gao, X.; Yue, Q.; Liu, Z.; Ke, M.; Zhou, X.; Li, S.; Zhang, J.; Zhang, R.; Chen, L.; Mao, Y.; Li, C. *Adv. Mater.* **2017**, *29*, 1603917.
- Landhuis, E. *Nature* **2017**, *551*, 257–259.
- Yao, L.; Song, Q.; Bai, W.; Zhang, J.; Miao, D.; Jiang, M.; Wang, Y.; Shen, Z.; Hu, Q.; Gu, X.; Huang, M.; Zheng, G.; Gao, X.; Hu, B.; Chen, J.; Chen, H. *Biomaterials* **2014**, *35*, 3384–3395.
- Fan, C.; Lin, C.; Liu, H.; Yeh, C. J. *Controlled Release* **2017**, *261*, 246–262.
- Mead, B. P.; Kim, N.; Miller, G. W.; Hodges, D.; Mastorakos, P.; Klivanov, A. L.; Mandell, J. W.; Hirsh, J.; Suk, J. S.; Hanes, J.; Price, R. J. *Nano Lett.* **2017**, *17*, 3533–3542.
- Yang, H.; Hua, M.; Hwang, T.; Lin, K.; Huang, C.; Tsai, R.; Ma, C. M.; Hsu, P.; Wey, S.; Hsu, P.; Chen, P.; Huang, Y.; Lu, Y.; Yen, T.; Feng, L.; Lin, C.; Liu, H.; Wei, K. *Adv. Mater.* **2013**, *25*, 3605–3611.
- Wu, M.; Chen, W.; Chen, Y.; Zhang, H.; Liu, C.; Deng, Z.; Sheng, Z.; Chen, J.; Liu, X.; Yan, F.; Zheng, H. *Adv. Sci.* **2018**, *5*, 1700474.
- Fan, C.; Ting, C.; Liu, H.; Huang, C.; Hsieh, H.; Yen, T.; Wei, K.; Yeh, C. *Biomaterials* **2013**, *34*, 2142–2155.
- Burgess, A.; Shah, K.; Hough, O.; Hynynen, K. *Expert Rev. Neurother.* **2015**, *15*, 477–491.
- Hynynen, K.; McDannold, N.; Vykhotseva, N.; Jolesz, F. A. *Radiology* **2001**, *220*, 640–646.
- Park, J.; Zhang, Y.; Vykhotseva, N.; Jolesz, F. A.; McDannold, N. *J. Controlled Release* **2012**, *162*, 134–142.
- Hynynen, K.; McDannold, N.; Sheikov, N. A.; Jolesz, F. A.; Vykhotseva, N. *NeuroImage* **2005**, *24*, 12–20.
- Cho, E. E.; Drazic, J.; Ganguly, M.; Stefanovic, B.; Hynynen, K. *J. Cereb. Blood Flow Metab.* **2011**, *31*, 1852–1862.
- Sheikov, N.; McDannold, N.; Sharma, S.; Hynynen, K. *Ultrasound in Med. Biol.* **2008**, *34*, 1093–1104.
- Nasr, S. H.; Kouyoumdjian, H.; Mallett, C.; Ramadan, S.; Zhu, D. C.; Shapiro, E. M.; Huang, X. *Small* **2018**, *14*, 1701828.
- Ruan, S.; Hu, C.; Tang, X.; Cun, X.; Xiao, W.; Shi, K.; He, Q.; Gao, H. *ACS Nano* **2016**, *10*, 10086–10098.
- Kircher, M. F.; de la Zerda, A.; Jokerst, J. V.; Zavaleta, C. L.; Kempen, P. J.; Mittra, E.; Pitter, K.; Huang, R.; Campos, C.; Habte, F.; Sinclair, R.; Brennan, C. W.; Mellinghoff, I. K.; Holland, E. C.; Gambhir, S. S. *Nat. Med.* **2012**, *18*, 829–834.
- Cheng, Y.; Morshed, R. A.; Auffinger, B.; Tobias, A. L.; Lesniak, M. S. *Adv. Drug Delivery Rev.* **2014**, *66*, 42–57.
- Kunjachan, S.; Ehling, J.; Storm, G.; Kiessling, F.; Lammers, T. *Chem. Rev.* **2015**, *115*, 10907–10937.
- Kim, S. E.; Zhang, L.; Ma, K.; Riegman, M.; Chen, F.; Ingold, I.; Conrad, M.; Turker, M. Z.; Gao, M.; Jiang, X.; Monette, S.; Pauliah, M.; Gonen, M.; Zanzonico, P.; Quinn, T.; Wiesner, U.; Bradbury, M. S.; Overholtzer, M. *Nat. Nanotechnol.* **2016**, *11*, 977–985.
- Mao, F.; Wen, L.; Sun, C.; Zhang, S.; Wang, G.; Zeng, J.; Wang, Y.; Ma, J.; Gao, M.; Li, Z. *ACS Nano* **2016**, *10*, 11145–11155.
- Wen, L.; Chen, L.; Zheng, S.; Zeng, J.; Duan, G.; Wang, Y.; Wang, G.; Chai, Z.; Li, Z.; Gao, M. *Adv. Mater.* **2016**, *28*, 5072–5079.
- Jiang, X.; Zhang, S.; Ren, F.; Chen, L.; Zeng, J.; Zhu, M.; Cheng, Z.; Gao, M.; Li, Z. *ACS Nano* **2017**, *11*, 5633–5645.
- Wang, Y.; Wu, Y.; Liu, Y.; Shen, J.; Lv, L.; Li, L.; Yang, L.; Zeng, J.; Wang, Y.; Zhang, L. W.; Li, Z.; Gao, M.; Chai, Z. *Adv. Funct. Mater.* **2016**, *26*, 5335–5344.
- Zhang, S.; Sun, C.; Zeng, J.; Sun, Q.; Wang, G.; Wang, Y.; Wu, Y.; Dou, S.; Gao, M.; Li, Z. *Adv. Mater.* **2016**, *28*, 8927–8936.
- Miao, Q.; Xie, C.; Zhen, X.; Lyu, Y.; Duan, H.; Liu, X.; Jokerst, J. V.; Pu, K. *Nat. Biotechnol.* **2017**, *35*, 1102.
- Kitagawa, K.; Matsumoto, M.; Tagaya, M.; Ueda, H.; Oku, N.; Kuwabara, K.; Ohtsuki, T.; Handa, N.; Kimura, K.; Kamada, T. *Acta Neuropathol.* **1991**, *82*, 164–171.

- (38) Li, J.; Xie, C.; Huang, J.; Jiang, Y.; Miao, Q.; Pu, K. *Angew. Chem., Int. Ed.* **2018**, *57*, 3995–3998.
- (39) Santiesteban, D. Y.; Dumani, D. S.; Profili, D.; Emelianov, S. Y. *Nano Lett.* **2017**, *17*, 5984–5989.
- (40) Jiang, Y.; Upputuri, P. K.; Xie, C.; Lyu, Y.; Zhang, L.; Xiong, Q.; Pramanik, M.; Pu, K. *Nano Lett.* **2017**, *17*, 4964–4969.
- (41) Yao, J.; Wang, L.; Yang, J.; Maslov, K. I.; Wong, T. T. W.; Li, L.; Huang, C.; Zou, J.; Wang, L. V. *Nat. Methods* **2015**, *12*, 407–410.
- (42) Li, L.; Zhu, L.; Ma, C.; Lin, L.; Yao, J.; Wang, L.; Maslov, K.; Zhang, R.; Chen, W.; Shi, J.; Wang, L. V. *Nat. Biomed. Eng.* **2017**, *1*, 0071.
- (43) Li, J.; Rao, J.; Pu, K. *Biomaterials* **2018**, *155*, 217–235.
- (44) Zhen, X.; Xie, C.; Jiang, Y.; Ai, X.; Xing, B.; Pu, K. *Nano Lett.* **2018**, *18*, 1498–1505.
- (45) Park, J.; Aryal, M.; Vykhodtseva, N.; Zhang, Y.; McDannold, N. *J. Controlled Release* **2017**, *250*, 77–85.
- (46) Favier, R. P.; Spee, B.; Fieten, H.; van den Ingh, T. S. G. A.; Schotanus, B. A.; Brinkhof, B.; Rothuizen, J.; Penning, L. C. *J. Trace Elem. Med. Biol.* **2015**, *29*, 347–353.
- (47) Prabhu, B. M.; Ali, S. F.; Murdock, R. C.; Hussain, S. M.; Srivatsan, M. *Nanotoxicology* **2010**, *4*, 150–160.
- (48) Iliiff, J. J.; Wang, M.; Liao, Y.; Plogg, B. A.; Peng, W.; Gundersen, G. A.; Benveniste, H.; Vates, G. E.; Deane, R.; Goldman, S. A.; Nagelhus, E. A.; Nedergaard, M. *Sci. Transl. Med.* **2012**, *4*, 147ra111.
- (49) Qi, J.; Fang, Y.; Kwok, R. T. K.; Zhang, X.; Hu, X.; Lam, J. W. Y.; Ding, D.; Tang, B. Z. *ACS Nano* **2017**, *11*, 7177–7188.
- (50) Zhang, X.; Chen, J.; Min, Y.; Park, G. B.; Shen, X.; Song, S.; Sun, Y.; Wang, H.; Long, W.; Xie, J.; Gao, K.; Zhang, L.; Fan, S.; Fan, F.; Jeong, U. *Adv. Funct. Mater.* **2014**, *24*, 1718–1729.